Editorial Manager(tm) for Developmental Cell
Manuscript Draft

Manuscript Number: DC-D-06-00013R1

Title: Mislocalization of the Drosophila centromere-specific histone CID promotes formation of functional ectopic kinetochores

Article Type: Research Article

Section/Category:

Keywords: centromere
CID
CENP-A
kinetochore
mitosis
aneuploidy

Corresponding Author: Dr. Gary H. Karpen,

Corresponding Author's Institution: Lawrence Berkeley National Lab/UC Berkeley

First Author: Patrick Heun, PhD

Order of Authors: Patrick Heun, PhD; Sylvia Erhardt, PhD; Michael D Blower, PhD; Samara Weiss, BA; Andrew D Skora, BA; Gary H Karpen, PhD

Manuscript Region of Origin:

Abstract: The centromere-specific histone variant CENP-A (CID in Drosophila) is a structural and functional foundation for kinetochore formation and chromosome segregation. Here, we show that overexpressed CID is mislocalized into normally non-centromeric regions in Drosophila tissue culture cells and animals. Analysis of mitoses in living and fixed cells reveals that mitotic delays, anaphase bridges, chromosome fragmentation, and cell and organismal lethality are all direct consequences of CID mislocalization. In addition, proteins that are normally restricted to endogenous kinetochores assemble at a subset of ectopic

CID incorporation regions. The presence of microtubule motors and binding proteins, spindle attachments, and aberrant chromosome morphologies demonstrate that these ectopic kinetochores are functional. We conclude that CID mislocalization promotes formation of ectopic centromeres and multicentric chromosomes, which causes chromosome missegregation, aneuploidy, and growth defects. Thus, CENP-A mislocalization is one possible mechanism for genome instability during cancer progression, as well as centromere plasticity during evolution.

Dear Debbie,

Thanks for your patience regarding submission of our manuscript revisions. We have successfully finished the requested experiments, and were able to address all of your issues and most of the reviewers comments. In our revised manuscript we have added the evaluation of proteins levels by Western blot to the results, as requested by Reviewer #2 (Supplemental Figure 1). As requested by the same reviewer, we also discussed the human study of CENP-A overexpression (Van Hooser et al.) in more detail. To address a major point raised by all reviewers, we provide additional examples of microtubule attachments to non-centromeric chromosome arms. These are now shown in an extended version of Figure 8, and Supplemental Movies S8-9, including co-localization with the outer kinetochore protein ROD. As explained previously, images with ectopic microtubule attachments are technically very difficult to obtain, which is why we quantitated mislocalization of the plus-end binding protein MAST (already a part of the previous manuscript).

The most significant addition to this manuscript is the simultaneous staining for different combinations of inner and outer kinetochore components. Not only do we observe significantly more sites of co-localization in CID-induced cells and animals, as compared to controls (1.4- to 2.8-fold), but we also find that most ectopic kinetochore sites recruit multiple kinetochore proteins. All the newly added co-localization data for S2 cells and imaginal discs are shown in Figure 6, and Tables 1 and 2.

We greatly appreciate the input provided by you and the reviewers, and believe that the additional experiments and text changes have greatly improved the manuscript. We hope you like the revised manuscript, and very much looking forward to hearing from you. One of us (PH) is applying for a Human Frontiers fellowship to fund his new lab; the due date is January 20th. If at all possible, it would be very helpful if you could decide on acceptance before then, in which case we would request a brief letter of acceptance that we could include in the application (HFSP requires such a letter for all ‘in press’ publications).

Best wishes,

Gary

*** Response to Reviewers**

Dear Debbie,

Thanks for your patience regarding submission of our manuscript revisions. We have successfully finished the requested experiments, and were able to address all of your issues and most of the reviewers comments. In our revised manuscript we have added the evaluation of proteins levels by Western blot to the results, as requested by Reviewer #2 (Supplemental Figure 1). As requested by the same reviewer, we also discussed the human study of CENP-A overexpression (Van Hooser et al.) in more detail. To address a major point raised by all reviewers, we provide additional examples of microtubule attachments to non-centromeric chromosome arms. These are now shown in an extended version of Figure 8, and Supplemental Movies S8-9, including co-localization with the outer kinetochore protein ROD. As explained previously, images with ectopic microtubule attachments are technically very difficult to obtain, which is why we quantitated mislocalization of the plus-end binding protein MAST (already a part of the previous manuscript).

The most significant addition to this manuscript is the simultaneous staining for different combinations of inner and outer kinetochore components. Not only do we observe significantly more sites of co-localization in CID-induced cells and animals, as compared to controls (1.4- to 2.8-fold), but we also find that most ectopic kinetochore sites recruit multiple kinetochore proteins. All the newly added co-localization data for S2 cells and imaginal discs are shown in Figure 6, and Tables 1 and 2.

We greatly appreciate the input provided by you and the reviewers, and believe that the additional experiments and text changes have greatly improved the manuscript. We hope you like the revised manuscript, and very much looking forward to hearing from you. One of us (PH) is applying for a Human Frontiers fellowship to fund his new lab; the due date is January 20th. If at all possible, it would be very helpful if you could decide on acceptance before then, in which case we would request a brief letter of acceptance that we could include in the application (HFSP requires such a letter for all ‘in press’ publications).

Best wishes,

Gary

Mislocalization of the Drosophila centromere-specific histone CID promotes formation of functional ectopic kinetochores

Patrick Heun,*[1,2,4] Sylvia Erhardt,*[1,2] Michael D. Blower,[2] Samara Weiss, [1,2] Andrew D. Skora[3] and Gary H. Karpen[1,2,5]

* These authors made equal contributions to this work.

[1] Department of Genome Biology, Lawrence Berkeley National Lab, One Cyclotron Road, Berkeley, CA 94720

[2] Department of Molecular and Cell Biology, University of California at Berkeley, Berkeley, CA 94720

[3] Department of Biology, Johns Hopkins University, 3400 N. Charles Street, Baltimore MD, 21208

[4] current address: MPI of Immunobiology, Stübeweg 5, Freiburg 79108, Germany

[\5] Correspondence: karpen@fruitfly.org

Summary
The centromere-specific histone variant CENP-A (CID in *Drosophila*) is a structural and functional foundation for kinetochore formation and chromosome segregation. Here, we show that overexpressed CID is mislocalized into normally non-centromeric regions in *Drosophila* tissue culture cells and animals. Analysis of mitoses in living and fixed cells reveals that mitotic delays, anaphase bridges, chromosome fragmentation, and cell and organismal lethality are all direct consequences of CID mislocalization. In addition, proteins that are normally restricted to endogenous kinetochores assemble at a subset of ectopic CID incorporation regions. The presence of microtubule motors and binding proteins, spindle attachments, and aberrant chromosome morphologies demonstrate that these ectopic kinetochores are functional. We conclude that CID mislocalization promotes formation of ectopic centromeres and multicentric chromosomes, which causes chromosome missegregation, aneuploidy, and growth defects. Thus, CENP-A mislocalization is one possible mechanism for genome instability during cancer progression, as well as centromere plasticity during evolution.

Introduction
Genome instability plays a key role in birth defects and cancer progression (Balmain et al., 2003). The centromeric DNA and chromatin is the most important chromosomal element required for segregation in mitosis and meiosis (Cleveland et al., 2003; Sullivan et al., 2001). In most eukaryotes there is only one centromere per chromosome, which is usually embedded in heterochromatin. The centromere and associated kinetochore are essential for microtubule spindle attachments, congression to the metaphase plate, anaphase segregation to the poles, and the function of the Mitotic Checkpoint (or Spindle Assembly Checkpoint, SAC). Centromere dysfunction results in chromosome loss due to the absence of spindle attachments, and chromosomes with more than one kinetochore (di- or multi-centrics) frequently fragment and missegregate, due to attachments of the same chromatid to both poles (McClintock, 1939).

Specification of only one site for centromere function (centromere identity) is regulated by epigenetic mechanisms in most eukaryotes (Cleveland et al., 2003; Sullivan et al., 2001). Transmissible dicentric chromosomes exist in which a kinetochore forms on only one of two regions of centromeric DNA, demonstrating that centromeric DNA is not sufficient for kinetochore formation (Agudo et al., 2000; Sullivan and Willard, 1998). Furthermore, centromeric DNA is not necessary for kinetochore formation, since non-centromeric DNA can acquire and faithfully propagate centromere proteins and functions (neocentromeres), without any change to the DNA sequences (Lo et al., 2001; Maggert and Karpen, 2001; Satinover et al., 2001). Finally, chromosome rearrangements are a hallmark of evolution and speciation, and are accompanied by centromere gains, losses, and movements with respect to genome sequences (Ferreri et al., 2005; Murphy and Karpen, 1998).

The CENP-A family of centromere-specific histone H3-like proteins serve as both structural and functional foundations for the kinetochore, and are excellent candidates for an epigenetic mark that establishes and propagates centromere identity (Cleveland et al., 2003; Sullivan et al., 2001). CENP-A proteins are constitutive chromatin components that are assembled into a cylindrical 3-D structure on mitotic chromosomes, around which the inner and outer kinetochore proteins are wrapped (Blower et al., 2002). They are essential for recruitment of kinetochore proteins, establishment of spindle attachments, and normal chromosome segregation in many eukaryotes (Blower and Karpen, 2001; Buchwitz et al., 1999; Chen et al., 2003; Howman et al., 2000; Stoler et al., 1995). In addition, reciprocal epistasis experiments have shown that CENP-A proteins are very high in the kinetochore

assembly pathway (Cleveland et al., 2003; Sullivan et al., 2001), consistent with CENP-A's location in chromatin at the base of the kinetochore (Blower et al., 2002).

CENP-A depletion provides one mechanism for generating aneuploidy in mitosis and meiosis, as well as centromere loss during evolution. In *Drosophila*, neocentromeres are generated due to proximity in *cis* to a functional, endogenous centromere, suggesting that spreading of key centromere chromatin proteins such as CENP-A is one molecular mechanism for centromere gain (Maggert and Karpen, 2001). However, the types of rearrangements observed during evolution or in human neocentromeric chromosomes indicate that *cis*-spreading cannot account for all cases of centromere gains.

Alternatively, centromere gain could also occur in response to CENP-A incorporation into normally non-centromeric regions, resulting in formation of ectopic kinetochores. Studies testing this hypothesis in mammals have produced ambiguous and contradictory results. In human tissue culture cells, overexpressed CENP-A was incorporated into non-centromeric regions, but did not appear to produce functional ectopic kinetochores (Van Hooser et al., 2001). In another study, 11 out of 11 human primary colorectal tumors sampled displayed CENP-A overexpression and mistargeting to normally noncentromeric regions, suggesting a potential link between CENP-A mislocalization and genome instability in cancer (Tomonaga et al., 2003).

Here, we directly test the hypothesis that CENP-A mislocalization into normally non-centromeric regions results in ectopic kinetochore formation. The effects of elevated levels of the *Drosophila* CENP-A homolog (CID) (Blower and Karpen, 2001; Henikoff et al., 2000) on cell and organismal proliferation and chromosome behavior were evaluated in both tissue culture cells and developing flies. Our results demonstrate that CID mislocalization can nucleate the formation of functional kinetochores at ectopic sites, which results in chromosome missegregation, aneuploidy, and growth defects.

Results

CID mislocalization results in growth defects in cells and animals

Stable *Drosophila* S2 cell lines were established that expressed either CID-GFP or Histone H3-GFP fusion proteins, under the control of the inducible metallothionein promoter. For studies in flies, we induced expression of transgenic CID-V5 or H3-V5 constructs using the GAL4-UAS system (Brand and Perrimon, 1993). Uninduced S2 cells or animals displayed leaky expression of the tagged CID proteins, which was exclusively targeted to endogenous centromeres (labeled 'control', Figure 1A), whereas leaky expression of tagged H3 was more broadly distributed in chromatin. Quantitative Western analysis indicated that CID-GFP induction in the whole population was 70-fold over endogenous CID levels (Supplemental Figure 1). However, subsequent functional analyses were performed on individual cells, which exhibited very different amounts of H3 and CID after induction (Figure 1A,B). Therefore, we quantitated protein levels in cells using GFP fluorescence; low, medium, and high levels of CID-GFP expression corresponded to approximately 10, 20, and 30-fold induction over control levels, respectively (see Experimental Procedures). Consistent with previous work (Collins et al., 2004; Henikoff et al., 2000; Van Hooser et al., 2001), overexpressed CID exhibited broad mislocalization in mitotic and polytene chromosomes, but was incorporated preferentially into euchromatin, with little if any signal visible in the pericentric heterochromatin (Figure 1C,D). Epitope-tagged H3 was also incorporated into chromatin, but predominantly localized to the heterochromatin.

Uninduced H3-GFP, CID-GFP, and untransfected S2 cells exhibited normal exponential growth, and untransfected S2 cell and H3-GFP cell growth was only slightly reduced after induction (Figure 2A). In contrast, overall cell growth was significantly reduced after CID-

GFP induction; specifically, cells expressing low, medium, and high levels of CID-GFP were quickly eliminated during culture, and cells with no or leaky CID-GFP levels eventually took over the population (Figure 2B). Ubiquitous and strong CID-V5 expression starting in early embryos (TUB-GAL-4 driver) resulted in abnormal development and lethality (Figure 2C). Another severe phenotype was observed with the EY-GAL4 driver; most of the adults displayed a reduced eye phenotype (85%) (Figure 2D), as observed previously (Jager et al., 2005). Analysis of mitotic indices and acridine orange staining showed that these phenotypes were caused by cell death or severe retardation of cell division (Supplemental Figure 2). None of these phenotypes were observed with overexpression of H3 or control levels of CID (Figure 2).

We conclude that CID mislocalization leads to mitotic arrest or severe delay, and cell death in S2 cells and animals, consistent with the observed phenotypes. In addition, the normal growth of control cells and animals demonstrates that the CID fusion proteins did not interfere with endogenous centromere function.

CID mislocalization causes severe chromosome segregation defects

Cytological analysis of mitosis was used to explore the cellular basis for the growth defects and lethality associated with CID overexpression and mislocalization. In fixed cells from S2 cultures, embryos, larval brains, and imaginal discs, CID incorporation into non-centromeric regions was associated with a variety of mitotic defects, including anaphase bridges, chromosomes stretched along the spindle axis, and chromosome fragmentation (Supplemental Figure 3). Similar mitotic abnormalities were observed in S2 cells overexpressing untagged CID, demonstrating that the defects were not due to the GFP fusion (data not shown). None of these defects were observed in controls, or in response to high levels of H3 expression.

Time-lapse analysis of mitosis in live S2 cells extended our understanding of the chromosomal defects displayed by cells with CID mislocalization. Most control cells (control CID-GFP or induced H3-GFP) displayed normal chromosome segregation during anaphase (Figure 3A, rows 1 and 2, Supplemental Movies S1 and 2, Figure 3C). CID overexpressing cells displayed significantly higher frequencies of lagging and abnormally stretched chromosomes (Figure 3A, row 3, Supplemental Movie S3, Figure 3C). Stretched chromosomes also produced fragments that failed to be incorporated into daughter nuclei (Figure 3A, row 4, Supplemental Movie S4). Finally, a substantially higher number of cells with induced CID-GFP expression displayed “cut” phenotypes, where chromosomes abnormally positioned near the spindle midzone in late anaphase were severed by the cleavage furrow during cytokinesis (Figure 3A, row 5, Supplemental Movie S5, Figure 3C).

Overall, time-lapse analysis revealed that mitotic defects were observed in 75% of cells with induced CID-GFP, compared to only ~18% of control cells (Figure 3D). Furthermore, even the lowest levels of induction produced significantly higher frequencies of mitotic abnormalities (55%) than controls, which were further elevated in cells with medium and high levels of expression (78% and 100%, respectively, Figure 3D). Thus, the frequency of mitotic abnormalities correlated with the amount of CID-GFP expression, suggesting that the defects are a direct result of CID mislocalization to normally non-centromeric regions. In addition, we frequently observed chromosomes that did not move in the typical V-form, as expected for a single spindle–chromosome attachment. Instead, chromosomes appeared to be stretched parallel to the spindle axis (Figure 3, rows 3 and 4, Figure 3C), a morphology consistent with spindle forces being applied to both chromosome arms, as observed for dicentric chromosomes (Ahmad and Golic, 1998). Finally, cells with induced CID-GFP displayed a three- to four-fold increase in the transition time between metaphase and anaphase onset (30.7 min) relative to control CID-GFP (7.5 min) or induced H3-GFP (10.8 min, $p<0.001$). These results demonstrate that CID mislocalization leads to significant

mitotic segregation defects, aneuploidy, and a delay in progression from metaphase to anaphase, which likely caused the observed growth defects and cell death.

CID mislocalization causes mitotic defects that differ from loss of endogenous centromere function or failure to separate sister chromatids

Although the chromosome morphologies and mitotic phenotypes imply that multicentric chromosomes form upon CID mislocalization, anaphase bridges and stretched chromosomes could also arise from defects in sister chromatid separation. In addition, lagging chromosomes could result from interference with endogenous centromere function. To address these possibilities, we performed time-lapse analysis of S2 cells with defective sister separation using the topoisomerase II inhibitor etoposide, and with cells depleted for CID by RNAi.

Etoposide treatment resulted in defects expected for inhibiting sister chromatid separation during anaphase (Chang et al., 2003; Coelho et al., 2003). Although centromeres moved normally and synchronously to the poles during anaphase, arms remained near the metaphase plate, producing massive bridges that were eventually 'cut' by cytokinesis (Figure 3B, row 1, Supplemental Movie S6). In addition, CID signals were stretched, consistent with previous observations suggesting that interlocking of sister chromatids elevates forces at kinetochores (Coelho et al., 2003).

The anaphase bridges formed after CID mislocalization were qualitatively and quantitatively different from failures in sister chromatid separation. After CID mislocalization, asynchronous poleward movement of centromeres and individual lagging chromosomes were observed, with no obvious centromere stretching (compare Supplemental Movies S3 and S6). Consistent with these differences, PROD, which binds a satellite DNA near the chromosomes 2 and 3 centromeres (Torok et al., 1997), was located predominantly near the poles after etoposide treatment, and telomeric HOAP antibody signals (Cenci et al., 2003) were enriched near the middle (Figure 4A, B). After CID mislocalization PROD signals were less frequently observed near the poles ($p<0.01$), and HOAP signals were less abundant near the middle ($p<0.025$). Finally, we only observed chromosomes stretched parallel to the spindle with endogenous centromeres at the center and telomeres oriented toward opposite poles after CID mislocalization, and not after etoposide treatment (Figure 4A, inset).

Similarly, the phenotypes observed after CID-depletion versus CID induction were significantly different. After CID RNAi, chromosomes did not congress to the metaphase plate, and displayed little movement toward the poles; no bridges were formed, and the chromosome mass that remained at the center was asymmetrically severed by cytokinesis (Figure 3B, row 2, Supplemental Movie S7). These differences were substantiated by the observation that PROD and HOAP were randomly distributed across the spindle after CID depletion, localizations that were distinct from those observed after CID mislocalization (Figure 4 A,B; $p<0.05$ and $p<0.01$, respectively).

We conclude that the CID mislocalization mitotic defects are phenotypically distinct from failure to resolve sister chromatid cohesion or loss of endogenous centromere function. Furthermore, phenotypes consistent with the presence of multiple kinetochores, such as stretched chromosomes with endogenous centromeres in the middle, were only observed after CID mislocalization.

Inner and outer kinetochore proteins are recruited to sites of ectopic CID incorporation

The hypothesis that ectopic kinetochores form in response to CID mislocalization was further tested by examining the distributions of proteins involved in centromeric chromatin and kinetochore functions. CENP-C is an inner kinetochore protein located between CENP-

A and outer kinetochore proteins in mitotic chromosomes (Blower et al., 2002), and is required for normal kinetochore formation (Sullivan et al., 2001). The Drosophila CENP-C homolog was recently shown to localize to centromeres in a CID-dependent manner (Jager et al., 2005), consistent with previous results in other organisms (Sullivan et al., 2001). Another protein associated with centromeric chromatin is MEI-S332 (Blower and Karpen, 2001; Kerrebrock et al., 1995), whose homologs (*shugoshins*) have recently been demonstrated to block degradation of centromeric cohesins (Kitajima et al., 2004; Salic et al., 2004). CID is required for normal MEI-S332 localization to the centromere region, whereas CID localization does not depend on MEI-S332 (Blower and Karpen, 2001). In order to examine effects on localization of an outer kinetochore protein, we stained cells for BUBR1, which is an outer kinetochore protein required for the mitotic checkpoint (Basu et al., 1998).

CENP-C, MEI-S332, and BUBR1 were localized exclusively to centromeres in S2 and fly imaginal disc cell controls (Figure 5); the number of spots was close to the amount expected for two sister kinetochores on the 13 ± 2 chromosomes present in S2 cells, and the 8 chromosomes in flies (Supplemental Tables 1 and 2). In contrast, significantly more sites (1.7- to 3.3-fold) were observed for all three proteins after CID induction, and the additional signals were located in normally non-centromeric (ectopic) regions (all p values <0.01). These differences were not due to elevated numbers of chromosomes in induced CID cells (data not shown).

To address whether individual ectopic sites of CID incorporation recruit multiple kinetochore proteins, we simultaneously stained control and induced cells with combinations of antibodies to different inner- and outer kinetochore proteins. Specifically, we quantitated colocalization of CENP-C/MEI-S332, CENP-C/POLO, POLO/ROD, MEI-S332/BUBR1 (Figure 6). POLO kinase strongly associates with the outer kinetochore from prometaphase through anaphase, and is required for spindle integrity and chromosome segregation (Logarinho and Sunkel, 1998). ROD is also localized to the outer kinetochore, and is required for recruitment of microtubule motors and normal segregation (Basto et al., 2000; Starr et al., 1998; Williams et al., 2003).

Normal CENP-C, MEI-S332, ROD, POLO and BUBR1 kinetochore localization was observed in control S2 and imaginal disc cells (Figure 6), and in cells with induced H3 (not shown). In contrast, all centromere/kinetochore proteins were mislocalized to significantly more ectopic sites in cells with CID mislocalization, in addition to endogenous centromeres (Figure 6, Supplemental Tables 1 and 2; all p values <0.01). As observed previously in single label experiments for CENP-C, MEI-S332, and BUBR1 (see above), ROD and POLO were present at 1.4- to 3.6-fold more sites after induction. Most importantly, all combinations of inner/inner, inner/outer, and outer/outer kinetochore proteins co-localized at significantly more sites after CID induction, compared to controls (1.4- to 2.8-fold; all p values <0.01). The percentage of centromere/kinetochore sites that contained both proteins after induction ranged from 39% to 85% in S2 cells, and 72% to 97% in disc cells, supporting the idea that most kinetochore proteins are recruited to the same ectopic sites.

These results demonstrate that CID mislocalization is associated with recruitment of multiple centromeric cohesion, inner kinetochore, and outer kinetochore proteins to normally non-centromeric sites, suggesting at least partial formation of ectopic kinetochores. Note that these proteins were not recruited to all sites of ectopic CID incorporation (see Discussion).

CID mislocalization results in the formation of functional ectopic kinetochores

The presence of ectopic centromere and kinetochore proteins, and the types of segregation defects, strongly suggests that ectopic kinetochores are formed after CID mislocalization. In order to evaluate the functionality of these ectopic kinetochores, we

determined whether kinetochore-associated microtubule motors and binding proteins, stable microtubule connections, and spindle-mediated forces were present at normally non-centromeric regions after CID mislocalization.

Chromosome movement is mediated by microtubule assembly and disassembly, and the functions of microtubule motors. The kinesin KLP59C is a microtubule depolymerizing protein located in the outer kinetochore, and is required for chromosome movement along spindles (Rogers et al., 2004). Dynein is a minus-end motor that links kinetochores to microtubules and contributes to poleward chromosome movement during anaphase A (Howell et al., 2001; Rogers et al., 2004). In mitosis, both Dynein and KLP59C were specifically associated with endogenous centromeres (and for Dynein on microtubules) in control CID-GFP cells, but colocalized at significantly more chromosomal sites after CID mislocalization, (2.3-fold increase, Supplemental Table 1, $p<0.02$).

Plus-end microtubule binding proteins, including Drosophila MAST, are concentrated at the interface between microtubules and functional kinetochores (Maiato et al., 2004; Maiato et al., 2002), providing an independent test for the presence of ectopic spindle attachments. Control S2 cells contained on average 26 MAST spots in metaphase, whereas cells with induced CID contained significantly more MAST spots (42, $p<0.001$, Figure 7 B,C). Similar results were obtained in flies; control imaginal disc cells contained 16 MAST spots in metaphase, compared to 35 spots after induction. In contrast, the number of MAST spots observed in etoposide-treated control S2 cells (28) was equivalent to the results from untreated control cells, and cells depleted for CID by RNAi contained only 6 MAST spots (Figure 7C). These results demonstrate that the number of functional ectopic kinetochore-microtubule attachments increases significantly specifically in cells with extensive CID mislocalization.

To visualize microtubule attachments, we exposed cells to cold treatment, which preferentially depolymerizes spindle microtubules that are not attached to kinetochores (Rieder, 1981). After CID induction, cells displayed cold-stable microtubule connections at ectopic sites that also contained CID and the outer kinetochore protein ROD (Figure 8A). 3D modeling demonstrated that microtubules ended at sites in the chromosome arms, far from the endogenous centromere (Supplemental Movies S8 and S9). In order to visualize ectopic microtubule attachments, we had to examined mis-segregating chromosomes (e.g. stretched) during late anaphase, when pole-to-pole microtubules are also retained after cold-treatment, which made quantitative comparisons difficult. However, such ectopic microtubule connections were never observed in S2 or imaginal disc cells overexpressing H3 or control levels of CID, or in S2 cells perturbed by CID depletion or etoposide treatment. In addition, the idea that these ectopic microtubule attachments exert force on the chromosome arms was supported by observations of stretched or bent chromosome arms with microtubule attachments to ectopic sites (Figure 8B, also see Figure 4A). Finally, the presence of significantly more ectopic sites containing the key kinetochore motors Dynein and KLP59C, and the plus-end binding protein MAST, provided quantitative evidence that ectopic spindle attachments were significantly increased after CID induction.

We conclude that CID induction results in ectopic chromosomal sites containing proteins implicated in forming functional microtubule attachments at kinetochores, as well as attachments similar to those found at endogenous kinetochores.

Discussion

Sites of ectopic CID incorporation are associated with kinetochore formation and function

CENP-A has been demonstrated to provide a structural and functional foundation for the kinetochore in a variety of organisms (Cleveland et al., 2003; Sullivan et al., 2001). This

study shows that ectopic incorporation of *Drosophila* CID into normally non-centromeric chromatin occurs in response to overexpression in S2 and animal cells, as observed previously in tissue culture cells and yeast (Collins et al., 2004; Henikoff et al., 2000; Van Hooser et al., 2001). Here, we show that CID mislocalization results in defective cell growth, cell and organismal death, and abnormal development.

Our results strongly support the conclusion that these mitotic abnormalities and growth defects are caused by formation of ectopic kinetochores and multiple spindle attachments on individual chromatids. First, studies of fixed and live cells demonstrated that CID overexpression caused significant mitotic defects, including increased mitotic index, and stretched, fragmented, and lagging chromosomes during anaphase. Time-lapse analysis in S2 cells revealed that CID overexpression also caused mitotic delays, as well as cut phenotypes, chromosome loss, and abnormal chromosome morphology during anaphase segregation.

Second, proteins that are normally associated with endogenous centromeres were present at ectopic sites in response to CID mislocalization. We examined the distribution and colocalization of proteins involved in different centromere / kinetochore structures and functions, extending from the centromeric chromatin to the outer kinetochore. Proteins associated with centromeric chromatin (CENP-C), centromeric cohesion (MEI-S332, BUBR1), outer kinetochore formation and motor protein recruitment (ROD, POLO), and the SAC (BUBR1) were mislocalized and colocalized to normally non-centromeric regions in S2 and animal cells with mislocalized CID. Thus, proteins involved in a wide spectrum of centromere and kinetochore functions are recruited together to ectopic sites after CID mislocalization.

Third, CID mislocalization resulted in significantly elevated numbers of sites containing the kinetochore-associated KLP59C and Dynein motor proteins, and the microtubule plus-end binding protein MAST. KLP59C and Dynein were frequently colocalized at normally non-centromeric regions of chromosomes that were displaying aberrant anaphase chromosome morphology. This data strongly suggests that ectopic CID incorporation can seed kinetochores that are able to form stable microtubule attachments, and that these attachments are able to transmit forces to chromosomes during mitosis. MAST localization in metaphase is likely to provide the best estimate for the number of ectopic functional kinetochores formed after CID induction, approximately twice the number observed in controls.

Finally, CID mislocalization resulted in the appearance of cold-stable microtubule attachments at normally non-centromeric regions, in addition to endogenous centromeres. The presence of ectopic spindle forces were confirmed in fixed preparations and time-lapse analysis by observing chromosomes with bent or stretched chromosome arms, which can only result from forces directing different sites on a single chromatid to the same pole. Likewise, in fixed cells and time-lapse analysis we observed chromosomes stretched along their longitudinal axes with endogenous centromeres in the middle, indicating that arms are under tension from opposite poles.

It is possible that other chromosome defects are caused by mislocalization of CID, in addition to ectopic kinetochore formation and multicentric chromosomes. However, inhibition of sister chromatid separation with the topoisomerase II inhibitor etoposide, and CID depletion by RNAi, produced mitotic defects that were qualitatively and quantitatively distinct from those observed after CID mislocalization. Thus, loss of endogenous centromere function or sister separation defects alone cannot account for the predominant chromosome phenotypes observed after CID mislocalization. Determining if other chromosome segregation defects in addition to ectopic kinetochores occurs in response to CID mislocalization warrants further study.

We conclude that CID induction results in broad incorporation into normally non-centromeric, predominantly euchromatic regions, a subset of which recruit key kinetochore proteins and exhibit kinetochore function. We propose that the mitotic, cellular, and organismal phenotypes are caused by the presence of more than one functional kinetochore and spindle attachments per chromatid. These results also provide further evidence that CENP-A is a key epigenetic mark for centromere identity (Sullivan et al., 2001).

Multiple factors regulate kinetochore formation at sites of CENP-A incorporation

Although CENP-A is currently the highest protein in the kinetochore assembly pathway, previous studies have not addressed whether CENP-A is also sufficient for kinetochore formation. The fact that most ectopic sites of CID incorporation were not associated with kinetochore proteins and spindle attachments indicates that CENP-A is not absolutely sufficient for kinetochore formation. However, there are several reasons why it is unlikely that a strict correlation between CENP-A incorporation and kinetochore formation would be observed in this system. First, it seems unlikely that all kinetochore proteins are present in the vast excess required for kinetochore formation at all ectopic CID sites. Interestingly, the inner kinetochore protein CENP-C was recruited more efficiently to ectopic sites in comparison to all the outer kinetochore proteins (Figures 5 and 6), suggesting that kinetochore formation may be limited by processes downstream from centromeric chromatin formation. Second, it is possible that only regions with CID incorporation above a threshold level, perhaps equivalent to the density at the endogenous centromere, are capable of establishing a functional kinetochore. This hypothesis is supported by the observation that the severity of chromosome segregation defects is closely correlated with CID expression levels. Lower levels of CENP-A induction is the most likely explanation for why ectopic kinetochores were not detected in the human study (Van Hooser et al., 2001). Alternatively human cells may possess a more efficient clearing mechanism for eliminating CENP-A from non-centromeric regions, as has been reported for *S. cerevisiae* (Collins et al., 2004). Third, other broadly distributed chromatin factors may contribute to functional kinetochore formation in combination with CID. Centromeric chromatin in flies and humans contains histone modification patterns that are distinct from euchromatin and the flanking heterochromatin, which may also be required for the formation of ectopic, functional kinetochores (Sullivan and Karpen, 2004).

Although centromere function and kinetochore assembly may require flanking heterochromatin, the presence of heterochromatin can also inhibit CID incorporation and kinetochore formation. In *Drosophila*, neocentromeres are produced when non-centromeric DNA and an endogenous centromere are juxtaposed, but not when heterochromatin separates these regions (Maggert and Karpen, 2001). The lack of CID incorporation into heterochromatin after induction is consistent with the hypothesis that heterochromatin antagonizes the spread of centromeric chromatin, and normally acts to limit the size and distribution of centromeric chromatin (Maggert and Karpen, 2000; Maggert and Karpen, 2001). Thus, differences in the distribution of heterochromatin may also limit CID incorporation into ectopic sites, or the ability of ectopic sites to form functional kinetochores. Further studies are needed to determine exactly what factors limit kinetochore formation at ectopic sites, and to examine the sufficiency of CENP-A in more detail.

CENP-A and genome instability

Studies in mammals, insects, and other lineages have shown that centromere gains and losses are a hallmark of chromosome evolution (Ferreri et al., 2005). Loss of an epigenetic mark such as CENP-A provides one mechanism for centromere inactivation without deletion of centromeric DNA. Identifying mechanisms for centromere gain is more

challenging, as it requires acquisition of an epigenetic mark in the absence of DNA sequence changes. Studies of experimentally induced neocentromeres in flies suggest one molecular mechanism for centromere gain, specifically *cis*-spreading of key centromere chromatin proteins such as CENP-A (Maggert and Karpen, 2001). However, this model cannot account for human neocentromere formation or most examples of centromere gain during evolution. The results presented here suggest a more appropriate mechanism for these cases of centromere acquisition, specifically CENP-A mislocalization, perhaps in response to transient overexpression. In addition, our results demonstrate that similar levels of CENP-A overexpression in Drosophila and human tumors (Tomonaga et al., 2003) can produce a spectrum of mitotic phenotypes consistent with the chromosome abnormalities observed in cancers (Balmain et al., 2003). Further investigations into the prevalence of CENP-A mislocalization in different types of human cancers, and its timing during cancer initiation and progression, are required to directly test this hypothesis.

Acknowledgments

We thank Roger Tsien for the mRFP construct, and the following people for antibodies: Roger Karess, Claudio Sunkel, David Sharp and Daniel Buster, Terry Orr-Weaver, Stefan Heideman, Tibor Török, and Jamy Peng. We also thank Abby Dernburg, Arshad Desai, Aaron Straight, and many lab members for discussions and critical reading of the manuscript, Pete Carlton for help with 3D modeling and Katie Freeman, David Acevedo, Cameron Kennedy, and Tomas Bogardus for general assistance. Funding for this research was provided by the Wellcome Trust to SE (072016), Deutsche Forschungsgemeinschaft (HE 3434/1-1) and Human Frontier Science Program (LT 00174/2002) to PH, and LBNL-LDRD (366987) and NIH R01 (GM 66272) grants to GK.

Experimental Procedures

Cloning and DNA constructs

Full-length H3 and CID were cloned into a modified pMT/V5 vector (Invitrogen), which contained an in-frame EGFP, and the hygromycin resistance gene Full-length histone H2B was inserted into a modified pIB/V5 vector (Invitrogen), which contained an in frame mRFP in the XhoI-SacII sites.

Cell culture

S2 cells were grown under standard conditions, and Ca Phosphate-DNA coprecipitation was used for transfection (Cherbas et al., 1994). Stable lines were selected and maintained using 100 mg/ml Hygromycin-B (Invitrogen). Protein expression was induced from the metallothionein promoter (pMT/V5 vectors) using 250 mM $CuSO_4$ for 24h.

Drosophila culture

Transgenic animals (Ashburner, 1990) were generated from the pP[UAST]CID-V5-6His or pP[UAST]H3-V5-6His constructs, which carry the mini-*white* gene. Several UAS-CID and UAS-H3 lines were established. Strong phenotypes were only observed at higher temperatures (28-29˚C). All 'UAS-driver lines' were obtained from the Bloomington stock center.

Cytological preparations and immunofluorescence

Unless otherwise noted, all S2 cells used for indirect IF were plated on Concanavalin-A (Sigma) coated slides, and processed as described (Henderson, 2004), except that cells stained for MAST were treated with 3µg/ml colcemid for 30 min. After fixation, all S2 cells

were processed for IF as described (Blower and Karpen, 2001), and mounted in SlowFade Light (Molecular Probes). Anti-tubulin staining was performed as described (Henderson, 2004), except that cells were cold-treated for 30 min at 4°C prior to fixation (Rieder, 1981). Cells were incubated with etoposide for 30 min, at a final concentration of 10 μM 2% DMSO . RNAi for CID was performed as described (Blower and Karpen, 2001).

Animal tissues were prepared and IF was performed as described (Henderson, 2004) except that tissues were prefixed for 1 min and incubated in 1mg/ml dispase/collagenase (Roche) for 5min prior to fixation. Mitotic chromosome and salivary gland squashes, and IF on embryos, were performed as described (Sullivan et al., 2000). IF for Tubulin was performed as described (Henderson, 2004), except that the tissues were incubated on ice for 1 min and fixation was carried out on ice. Embryos and disc cells were mounted in Vectashield (Vector Laboratories) containing DAPI.

For IF of both S2 cells and animal tissues, dilutions for the CID, ROD, POLO, TUBULIN, BUBR1, PROD, and MEI-S332 primary antibodies were as described (Blower and Karpen, 2001). Dilutions for other primary antibodies were mouse anti-V5 (1:500), rabbit anti-H3 Ser10 (1:250), guinea pig anti-HOAP (1:100) rabbit anti-KLP59C (1:500), mouse anti-Dynein (1:500), rabbit anti-MAST (1:10), and rabbit anti-CENP-C (1:5000). Secondary antibodies were coupled to Alexa 488, Alexa 546 and Alexa 647 fluorophores (Molecular Probes), and were used at 1:500 dilutions.

Microscopy

All images were taken on a Deltavision Spectris® Microscope and deconvolved using softWoRx® (Applied Precision). For indirect IF, images were taken as z-stacks of 0.2 μm increments, using a 100x oil-immersion objective. For the growth rate and protein expression studies, 10 z-stacks of 1 μm increments were taken on a 40x oil-immersion objective quick projected and quantified for GFP levels using arbitrary density units. For time-lapse microscopy, 10 μl of exponentially growing cultures were added to a cover slip and processed as described using the “hanging drop” method (Shields and Sang, 1970). Seven z-stacks of 1 μm increments were captured for each channel (GFP, RFP and transmission light) at 1 frame/min using a 60x oil-immersion objective. Movies are displayed as quick projections and GFP levels of metaphase plates were quantified using softWoRx®. Fold-induction of CID-GFP expression in S2 cells was quantified using the sum of pixel intensity in the different z-sections for the first picture of each time-lapse movie for both induced- and uninduced cells, and categorized as control (uninduced)= <14, low=90-190, medium=190-290, and high= >290. Images of flies, heads and pupae cases were taken on a dissecting microscope with a Polaroid CCD camera, and analyzed with the DMC direct software. All statistical comparisons of the numbers of localization sites utilized the Mann-Whitney U Test.

References

Agudo, M., Abad, J. P., Molina, I., Losada, A., Ripoll, P., and Villasante, A. (2000). A dicentric chromosome of Drosophila melanogaster showing alternate centromere inactivation. Chromosoma *109*, 190-196.

Ahmad, K., and Golic, K. G. (1998). The transmission of fragmented chromosomes in Drosophila melanogaster. Genetics *148*, 775-792.

Ashburner, M. (1990). Drosophila: A Laboratory Handbook (Cold Spring Harbor: Cold Spring Harbor Press).

Balmain, A., Gray, J., and Ponder, B. (2003). The genetics and genomics of cancer. Nat Genet *33 Suppl*, 238-244.

Basto, R., Gomes, R., and Karess, R. E. (2000). Rough deal and Zw10 are required for the metaphase checkpoint in Drosophila. Nat Cell Biol *2*, 939-943.
Basu, J., Logarinho, E., Herrmann, S., Bousbaa, H., Li, Z., Chan, G. K., Yen, T. J., Sunkel, C. E., and Goldberg, M. L. (1998). Localization of the Drosophila checkpoint control protein Bub3 to the kinetochore requires Bub1 but not Zw10 or Rod. Chromosoma *107*, 376-385.
Blower, M. D., and Karpen, G. H. (2001). The role of Drosophila CID in kinetochore formation, cell-cycle progression and heterochromatin interactions. Nature Cell Biology *3*, 730-739.
Blower, M. D., Sullivan, B. A., and Karpen, G. H. (2002). Conserved organization of centromeric chromatin in flies and humans. Dev Cell *2*, 319-330.
Brand, A. H., and Perrimon, N. (1993). Targeted gene expression as a means of altering cell fates and generating dominant phenotypes. Development *118*, 401-415.
Buchwitz, B. J., Ahmad, K., Moore, L. L., Roth, M. B., and Henikoff, S. (1999). A histone H3-like protein in *C. elegans*. Nature *401*, 547.
Cenci, G., Siriaco, G., Raffa, G. D., Kellum, R., and Gatti, M. (2003). The Drosophila HOAP protein is required for telomere capping. Nat Cell Biol *5*, 82-84.
Chang, C. J., Goulding, S., Earnshaw, W. C., and Carmena, M. (2003). RNAi analysis reveals an unexpected role for topoisomerase II in chromosome arm congression to a metaphase plate. J Cell Sci *116*, 4715-4726.
Chen, E. S., Saitoh, S., Yanagida, M., and Takahashi, K. (2003). A cell cycle-regulated GATA factor promotes centromeric localization of CENP-A in fission yeast. Mol Cell *11*, 175-187.
Cherbas, L., Moss, R., and Cherbas, P. (1994). Transformation techniques for Drosophila cell lines. Methods Cell Biol *44*, 161-179.
Cleveland, D. W., Mao, Y., and Sullivan, K. F. (2003). Centromeres and kinetochores: from epigenetics to mitotic checkpoint signaling. Cell *112*, 407-421.
Coelho, P. A., Queiroz-Machado, J., and Sunkel, C. E. (2003). Condensin-dependent localisation of topoisomerase II to an axial chromosomal structure is required for sister chromatid resolution during mitosis. J Cell Sci *116*, 4763-4776.
Collins, K. A., Furuyama, S., and Biggins, S. (2004). Proteolysis contributes to the exclusive centromere localization of the yeast Cse4/CENP-A histone H3 variant. Curr Biol *14*, 1968-1972.
Ferreri, G. C., Liscinsky, D. M., Mack, J. A., Eldridge, M. D., and O'Neill, R. J. (2005). Retention of latent centromeres in the Mammalian genome. J Hered *96*, 217-224.
Henderson, D. S. (2004). Visualizing Mitosis in Whole-Mount Larval Brains, In Drosophila Cytogenetics Protocols, D. S. Henderson, ed. (Totowa, N.J.: Humana Press), pp. 363-371.
Henikoff, S., Ahmad, K., Platero, J. S., and van Steensel, B. (2000). Heterochromatic deposition of centromeric histone H3-like proteins. Proc Natl Acad Sci U S A *97*, 716-721.
Howell, B. J., McEwen, B. F., Canman, J. C., Hoffman, D. B., Farrar, E. M., Rieder, C. L., and Salmon, E. D. (2001). Cytoplasmic dynein/dynactin drives kinetochore protein transport to the spindle poles and has a role in mitotic spindle checkpoint inactivation. J Cell Biol *155*, 1159-1172.
Howman, E. V., Fowler, K. J., Newson, A. J., Redward, S., MacDonald, A. C., Kalitsis, P., and Choo, K. H. (2000). Early disruption of centromeric chromatin organization in centromere protein A (Cenpa) null mice. Proc Natl Acad Sci U S A *97*, 1148-1153.
Jager, H., Rauch, M., and Heidmann, S. (2005). The Drosophila melanogaster condensin subunit Cap-G interacts with the centromere-specific histone H3 variant CID. Chromosoma *113*, 350-361.
Kerrebrock, A. W., Moore, D. P., Wu, J. S., and Orr-Weaver, T. L. (1995). Mei-S332, a Drosophila protein required for sister-chromatid cohesion, can localize to meiotic centromere regions. Cell *83*, 247-256.

Kitajima, T. S., Kawashima, S. A., and Watanabe, Y. (2004). The conserved kinetochore protein shugoshin protects centromeric cohesion during meiosis. Nature *427*, 510-517.
Lo, A. W. I., Magliano, D. J., Sibson, M. C., Kalitsis, P., Craig, J. M., and Choo, K. H. A. (2001). A novel chromatin immunoprecipitation and array (CIA) analysis identifies a 460-kb CENP-A-binding neocentromere DNA. Genome Res *11*, 448-457.
Logarinho, E., and Sunkel, C. E. (1998). The Drosophila POLO kinase localises to multiple compartments of the mitotic apparatus and is required for the phosphorylation of MPM2 reactive epitopes. J Cell Sci *111*, 2897-2909.
Maggert, K. A., and Karpen, G. H. (2000). Acquisition and metastability of centromere identity and function: sequence analysis of a human neocentromere. Genome Res *10*, 725-728.
Maggert, K. A., and Karpen, G. H. (2001). Neocentromere formation occurs by an activation mechanism that requires proximity to a functional centromere. Genetics *158*, 1615-1628.
Maiato, H., DeLuca, J., Salmon, E. D., and Earnshaw, W. C. (2004). The dynamic kinetochore-microtubule interface. J Cell Sci *117*, 5461-5477.
Maiato, H., Sampaio, P., Lemos, C. L., Findlay, J., Carmena, M., Earnshaw, W. C., and Sunkel, C. E. (2002). MAST/Orbit has a role in microtubule-kinetochore attachment and is essential for chromosome alignment and maintenance of spindle bipolarity. J Cell Biol *157*, 749-760.
McClintock, B. (1939). The behaviour of successive nuclear divisions of a chromosome broken at meiosis. Proc Natl Acad Sci USA *25*, 405-416.
Murphy, T. D., and Karpen, G. H. (1998). Centromeres take flight: alpha satellite and the quest for the human centromere. Cell *93*, 317-320.
Rieder, C. L. (1981). The structure of the cold-stable kinetochore fiber in metaphase PtK1 cells. Chromosoma *84*, 145-158.
Rogers, G. C., Rogers, S. L., Schwimmer, T. A., Ems-McClung, S. C., Walczak, C. E., Vale, R. D., Scholey, J. M., and Sharp, D. J. (2004). Two mitotic kinesins cooperate to drive sister chromatid separation during anaphase. Nature *427*, 364-370.
Salic, A., Waters, J. C., and Mitchison, T. J. (2004). Vertebrate shugoshin links sister centromere cohesion and kinetochore microtubule stability in mitosis. Cell *118*, 567-578.
Satinover, D. L., Vance, G. H., Van Dyke, D. L., and Schwartz, S. (2001). Cytogenetic analysis and construction of a BAC contig across a common neocentromeric region from 9p. Chromosoma *110*, 275-283.
Shields, G., and Sang, J. H. (1970). Characteristics of five cell types appearing during in vitro culture of embryonic material from Drosophila melanogaster. J Embryol Exp Morphol *23*, 53-69.
Starr, D. A., Williams, B. C., Hays, T. S., and Goldberg, M. L. (1998). ZW10 helps recruit dynactin and dynein to the kinetochore. J Cell Biol *142*, 763-774.
Stoler, S., Keith, K. C., Curnick, K. E., and Fitzgerald-Hayes, M. (1995). A mutation in CSE4, an essential gene encoding a novel chromatin-associated protein in yeast, causes chromosome nondisjunction and cell cycle arrest at mitosis. Genes Dev *9*, 573-586.
Sullivan, B. A., Blower, M. D., and Karpen, G. H. (2001). Determining Centromere Identity: Cyclical Stories and Forking Paths. Nature Reviews Genetics *2*, 584-596.
Sullivan, B. A., and Karpen, G. H. (2004). Centromeric chromatin exhibits a histone modification pattern that is distinct from both euchromatin and heterochromatin. Nat Struct Mol Biol *11*, 1076-1083.
Sullivan, B. A., and Willard, H. F. (1998). Stable dicentric X chromosomes with two functional centromeres. Nat Genet *20*, 227-228.
Sullivan, W., Ashburner, M., and Hawley, R. S. (2000). Drosophila protocols (Cold Spring Harbor, N.Y.: Cold Spring Harbor Press).

Tomonaga, T., Matsushita, K., Yamaguchi, S., Oohashi, T., Shimada, H., Ochiai, T., Yoda, K., and Nomura, F. (2003). Overexpression and mistargeting of centromere protein-A in human primary colorectal cancer. Cancer Res *63*, 3511-3516.
Torok, T., Harvie, P. D., Buratovich, M., and Bryant, P. J. (1997). The product of proliferation disrupter is concentrated at centromeres and required for mitotic chromosome condensation and cell proliferation in Drosophila. Genes Dev *11*, 213-225.
Van Hooser, A. A., Ouspenski, II, Gregson, H. C., Starr, D. A., Yen, T. J., Goldberg, M. L., Yokomori, K., Earnshaw, W. C., Sullivan, K. F., and Brinkley, B. R. (2001). Specification of kinetochore-forming chromatin by the histone H3 variant CENP-A. J Cell Sci *114*, 3529-3542.
Williams, B. C., Li, Z., Liu, S., Williams, E. V., Leung, G., Yen, T. J., and Goldberg, M. L. (2003). Zwilch, a new component of the ZW10/ROD complex required for kinetochore functions. Mol Biol Cell *14*, 1379-1391.

Figure Legends

Figure 1 CID-GFP or H3-GFP expressing S2 cells display different protein levels and localizations upon induction. **(A)** H3-GFP staining was widely distributed in the nucleus at all levels of expression, whereas CID-GFP staining patterns depended on expression levels: centromere only (low), diffuse plus centromere (medium), and diffuse (high). **(B)** CID overexpression in animals carrying UAS-CID-V5. IF using anti-CID antibodies (green) on eye-antenna discs show that the EY-GAL4 driver is very specific to the eye disc. The levels of CID varied from low (L), medium (M), to high (H). Cells in the antenna disc display endogenous CID levels. **(C)** Distribution of H3-GFP/ H3-V5 (top images) and low and high levels of CID-GFP/CID-V5 (green: GFP or V5 antibodies) on metaphase chromosomes from S2 cells (left), and from larval discs (right). High CID-GFP/CID-V5 staining is predominantly euchromatic and at endogenous centromeres (green arrows), and is not extensively incorporated into pericentric heterochromatin (blue bars), unlike H3-GFP/H3-V5. **(D)** CID (green) was abnormally incorporated into polytene chromosome arms, bands (white arrow), and telomeres (asterisk) after heat shock induction of larvae containing HSP70-GAL4 and UAS-CID-V5. Only low levels of CID-V5 were incorporated into the heterochromatic chromocenter (CC). Scale bars, 5 μm in **C** and 15 μm in **D**.

Figure 2 CID overexpression results in cellular and organismal phenotypes. **(A)** Growth curves are shown for untransfected or stably transfected S2 cells carrying CID-GFP or H3-GFP, with and without $CuSO_4$ induction. Induced CID-GFP cells displayed significant growth defects from day 8 to 12. **(B)** H3-GFP expressing cells maintained a similar distribution of protein levels once fully induced (~day 4), whereas the percentage of cells with CID-GFP levels above 150 decreased significantly after day 4. **(C)** Ubiquitous CID induction resulted in organismal lethality (96%, n=305). The majority (76%,) stopped developing before pupariation (left panel), and 20% metamorphosed but were unable to hatch (right panel). The few flies (4%) that hatched, as well as the unhatched pupae, were substantially smaller than control flies. **(D)** Eye-specific CID induction resulted in strongly reduced eye size (lower panel) in comparison to controls (upper panel). Approximately 85% of induced flies (n=391) showed a severe visible phenotype (histogram).

Figure 3 Time-lapse analysis of live S2 cells reveals mitotic defects after CID induction (see Supplemental Movies). **(A)** Frames from time-lapse microscopy are shown for induced H3-GFP, control CID-GFP co-expressed with H2B-RFP (chromosome counter stain), and

induced CID-GFP. Phase indicates cell outlines. Control chromosomes segregate normally. In contrast, cells with induced CID-GFP expression displayed stretched chromosomes, fragmentation (asterisk, inset) and 'cutting' of the unsegregated chromosome mass by cytokinesis (see **(C)** for quantitation). **(B)** Cells were treated with Etoposide to mimic problems in resolving sister chromatids (row 6), or were depleted for CID by RNAi (row 7), and displayed distinct segregation defects in comparison to CID mislocalization. Scale bars, 5 μm. **(C)** Quantitation of defects observed in the time-lapse analysis. Cells induced for CID-GFP displayed higher percentages of all types of mitotic defects (induced $n_{H3\text{-}GFP}$=32, $n_{CID\text{-}GFP\ control}$=50, $n_{induced\ CID\text{-}GFP}$=27). For all phenotypes the differences were highly significant ($p<0.001$, Chi square test). **(D)** Levels of CID-GFP expression correlated with a highly elevated overall frequency of defective mitoses and all are significantly different from the controls ($p<0.01$, in comparison to controls; H3-GFP: n=32, control: n= 50, CID-GFP, low: n=11, medium: n=9 and high: n=7).

Figure 4 CID mislocalization causes mitotic defects that are different from failure to separate sister chromatids or the loss of endogenous centromere function. **(A)** Induced S2 cells, and uninduced cells treated with Etoposide or depleted for CID (CID RNAi) were fixed and stained for CID (green), PROD (red), and HOAP (blue). The inset shows a frequently observed phenotype of a chromosome (asterisk) being stretched along its length axis, with the centromeres (PROD) positioned in the middle, and the telomeres (HOAP) facing opposite poles. **(B)** The distance of all PROD (endogenous centromere) and HOAP (telomere) foci from the two poles were measured, normalized to the length of the cell, and expressed as percent distance from the pole (see ruler, bottom left in A). Cells with induced CID expression had PROD spots positioned less frequently near the poles and fewer HOAP spots in the middle, compared to Etoposide treatment. Cells depleted for CID display random staining for both. Note that 2 of 10 PROD spots per cell colocalized with HOAP, and were omitted from the quantitation. Scale bars, 5 μm.

Figure 5 Induction of ectopic CID results in aberrant localization of centromere and kinetochore proteins to normally non-centromeric regions. Localization of the inner kinetochore protein CENP-C, the sister cohesion protein MEI-S332, and BUBR1. CENP-C, MEI-S332 and BUBR1 are in red, CID-GFP in S2 cells and CID-V5 in larval disc cells are in green. Enlargements of individual chromosomes of S2 cells are shown below; green arrows = endogenous centromeres, white arrows = ectopic sites. Normal centromeric localization of all three proteins was observed in controls. Upon CID induction, these proteins were abnormally localized to many non-centromeric sites, and the average number of sites (below) was significantly higher in induced versus control cells ($p<0.01$, Supplemental Tables 1 and 2). Scale bars, 5 μm.

Figure 6 Inner and outer kinetochore proteins colocalize at sites of ectopic CID incorporation. Control and induced cells were simultaneously stained with CENP-C/MEI-S332, CENP-C/POLO, POLO/ROD, or MEI-S332/BUBR1 antibodies. CID-GFP in S2 cells and CID-V5 in larval disc cells are in green, CENP-C and ROD are in red, and POLO and MEI-S332 are in blue. Enlargements of individual chromosomes of S2 cells are shown below. Inner and outer kinetochore proteins were often colocalized at ectopic sites (white arrows), in addition to the endogenous centromeres (green arrows). The average number of colocalization sites (below) was significantly higher in induced versus control cells ($p<0.01$, Supplemental Tables 1 and 2). Scale bars, 5 μm.

Figure 7 Distributions of microtubule motors and the plus-end binding protein MAST suggest the presence of functional ectopic kinetochores. **(A)** Localization of the motor

proteins Dynein and kinesin KLP59C. Merged images for anaphase figures are shown on top, and enlargements are shown below. CID-GFP expressing cells were stained for CID (green), Dynein and KLP59C (blue). Control cells display close association of both proteins only at endogenous centromeres (green arrows), whereas they frequently colocalize at ectopic chromosomal sites (white arrow) after induction (average number of sites indicated below, see Supplemental Table 1). Note that Dynein also decorates underlying spindle microtubules (asterisk). Scale bars, 5 μm. **(B)** Localization of the microtubule plus-end binding protein MAST. Metaphase figures from induced cells contain more MAST (red) spots than observed in controls. Scale bars, 5 μm. **(C)** Quantitation of MAST spots in S2 and imaginal disc cells. MAST signals associated with spindle poles (asterisk in B) were not included in the quantitation. Induced cells contained significantly elevated numbers of MAST spots compared to controls (p values in text). Etoposide treatment did not alter the number of MAST spots from control values, and CID depletion by RNAi resulted in significantly fewer MAST spots than controls ($p<0.001$ for I or CID RNAi vs. C; S2 cells: $n_C=19$, $n_I=17$, $n_{ETOP}=16$, $n_{CID\ RNAi}=14$, Imaginal disks: $n_C=12$, $n_I=13$).

Figure 8 Ectopic microtubule attachments and aberrant chromosome morphologies are observed after CID induction. **(A)** Anaphase figure from CID-GFP expressing S2 cells (higher magnification to the right) display prominent ectopic CID-GFP foci (white arrows) connected to microtubule bundles (red), and colocalized with ROD (light blue), far from the endogenous centromere (asterisk). **(B)** Chromosome morphologies suggest poleward forces applied to chromosome arms after CID induction. The panel to the right shows enlargements of chromosomes, plus a schematic interpretation of the forces (red arrows) responsible for the observed chromosome morphologies. Scale bars, 5 μm.

Figure 1

Click here to download high resolution image

Figure 1

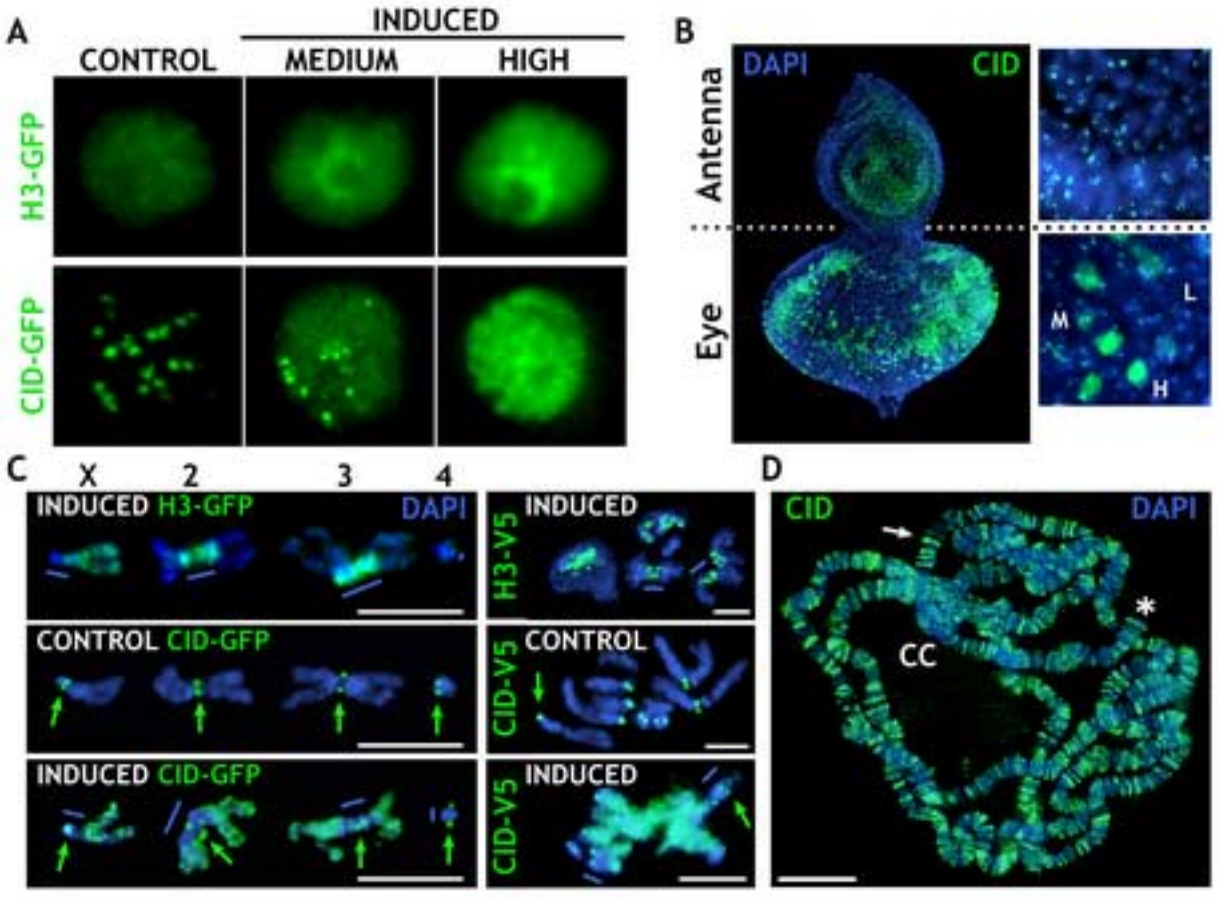

Figure 2

Click here to download high resolution image

Figure 2

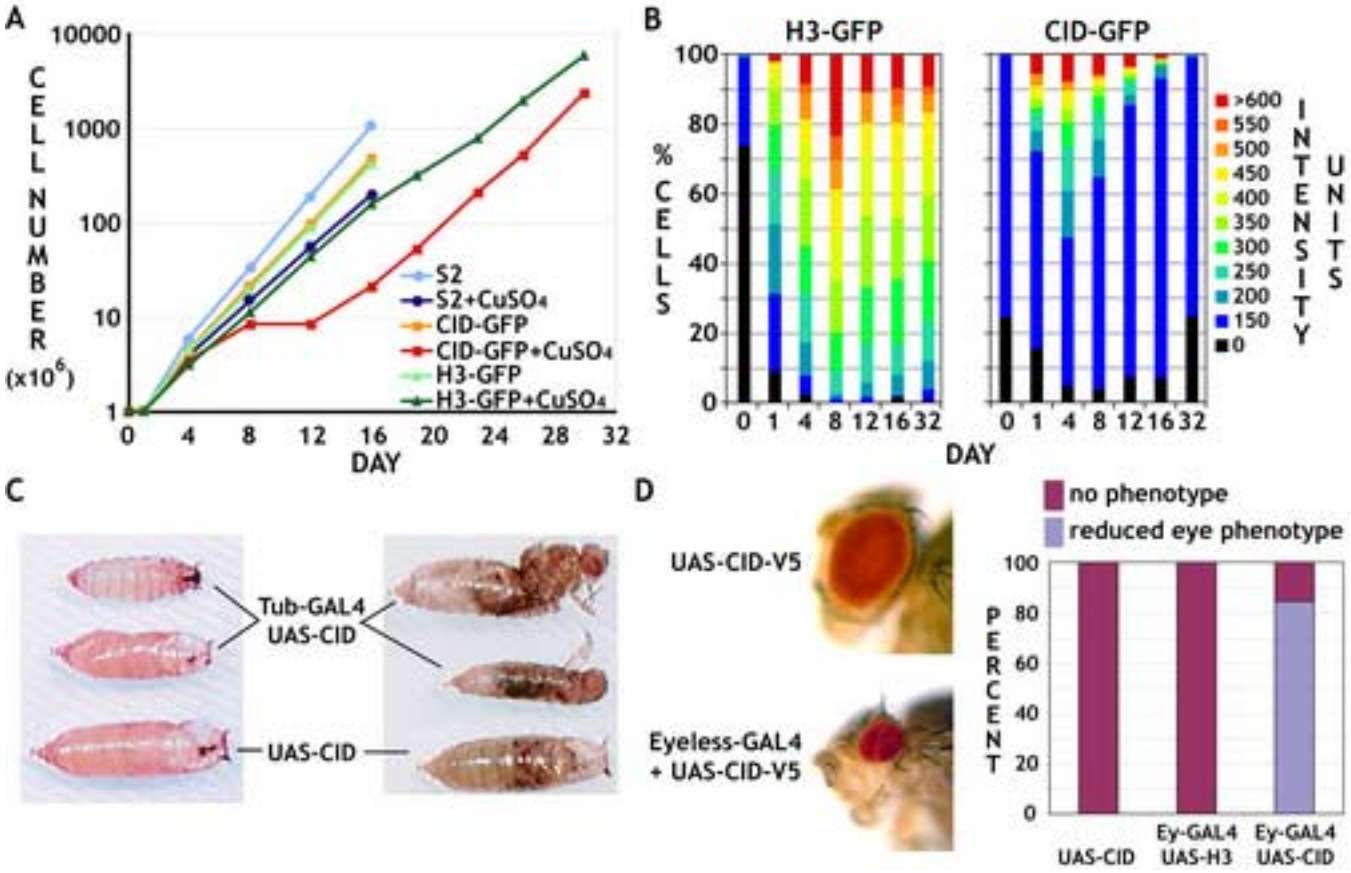

Figure 3

Click here to download high resolution image

Figure 3

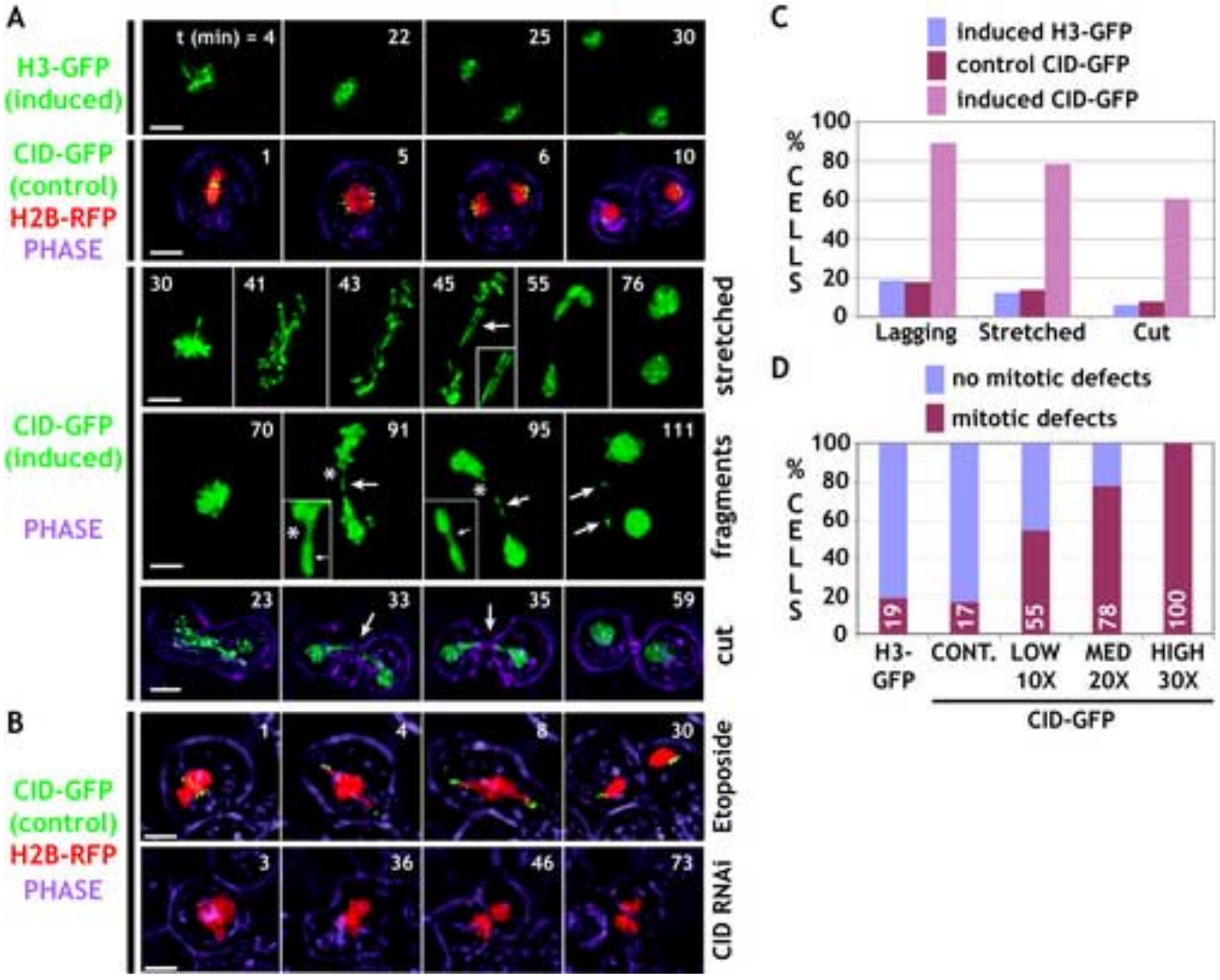

Figure 4

Click here to download high resolution image

Figure 4

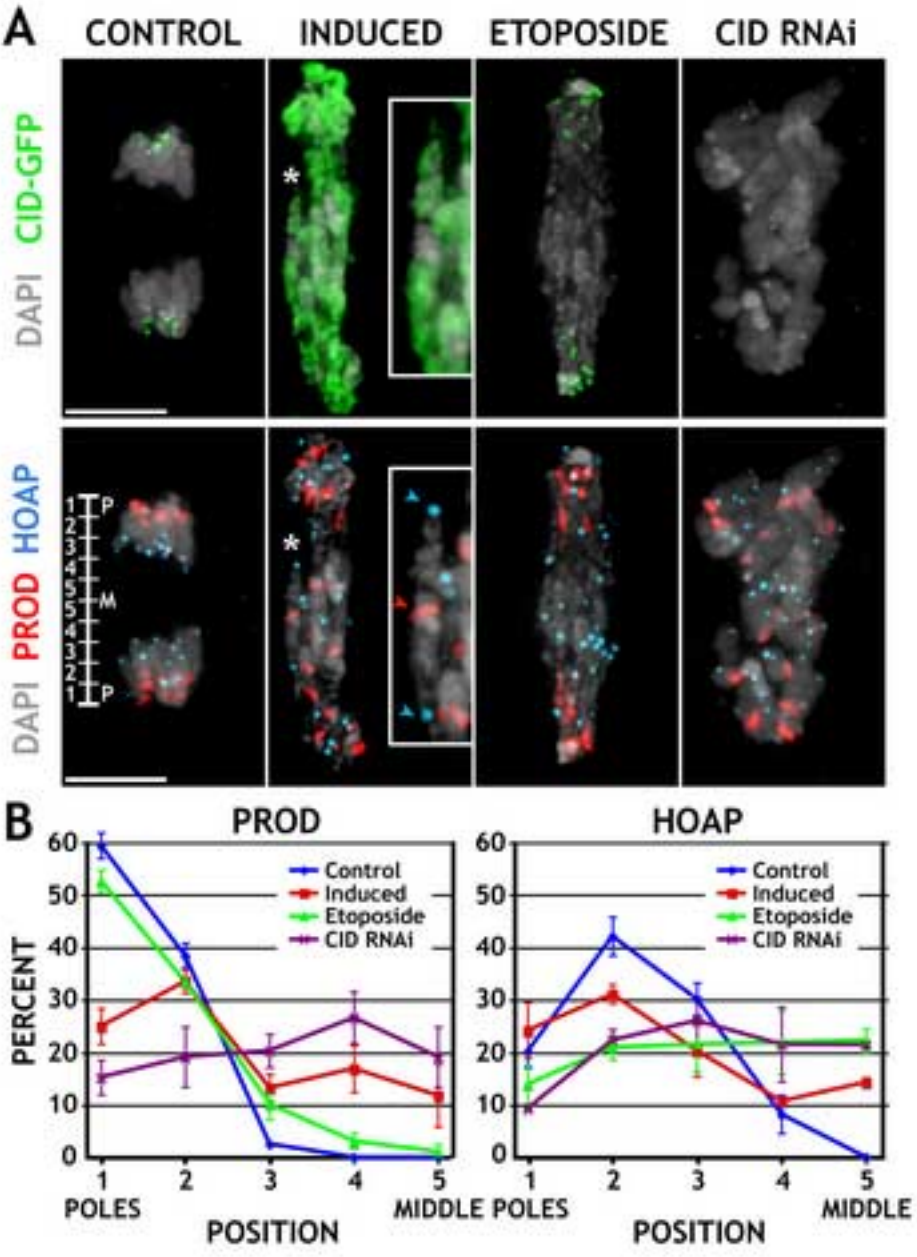

Figure 5

Click here to download high resolution image

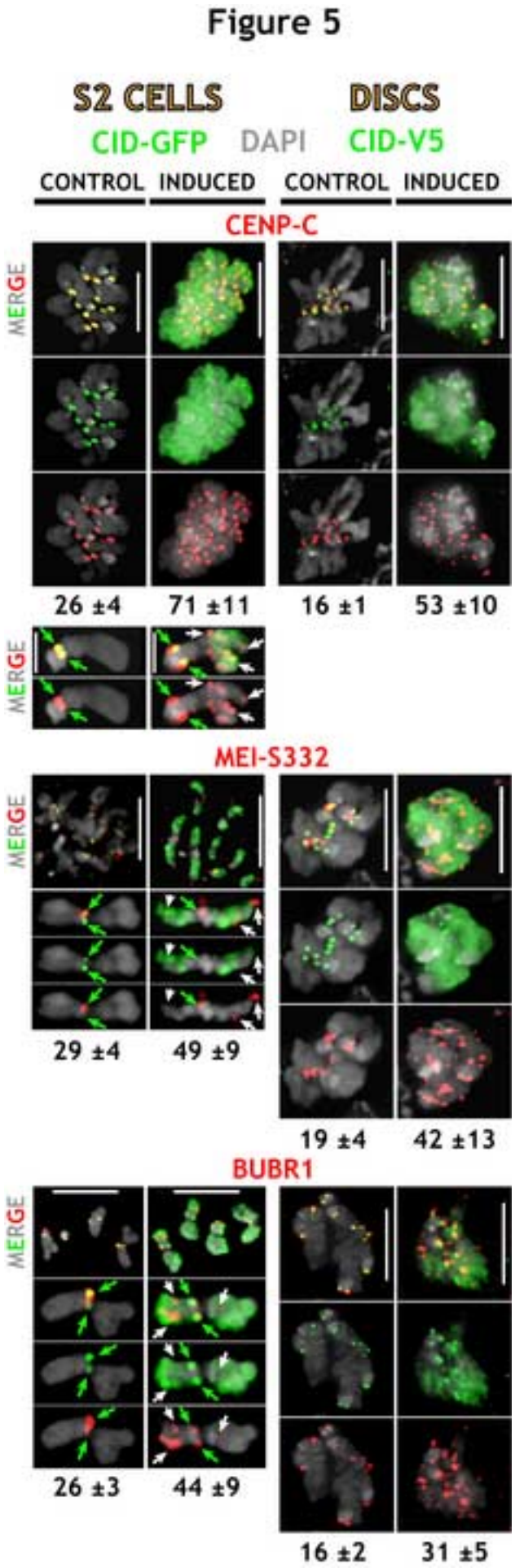

Figure 6

Click here to download high resolution image

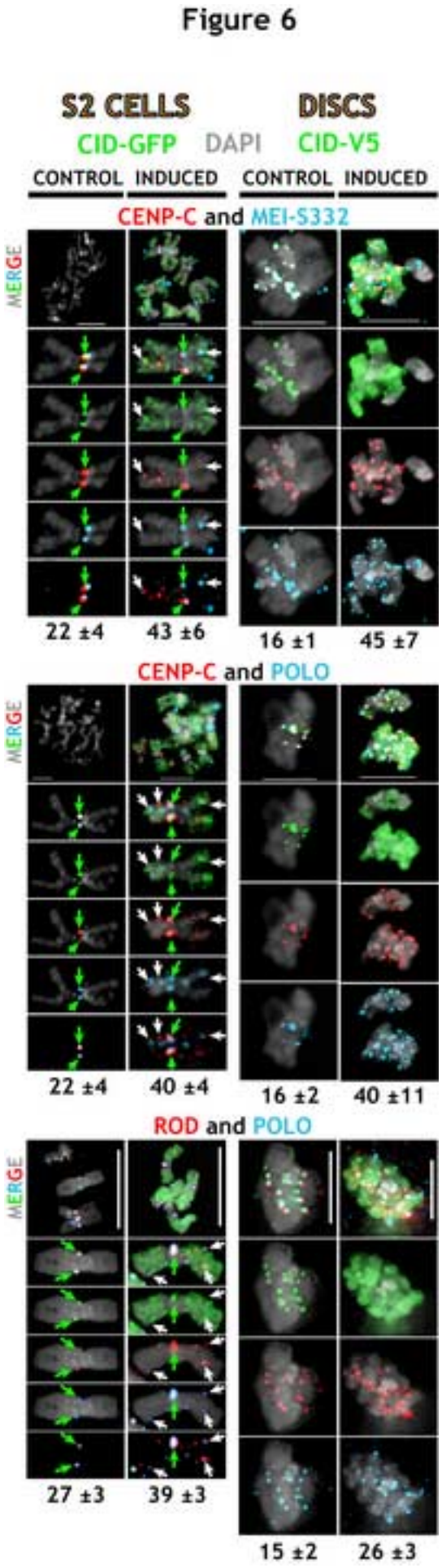

Figure 7

Click here to download high resolution image

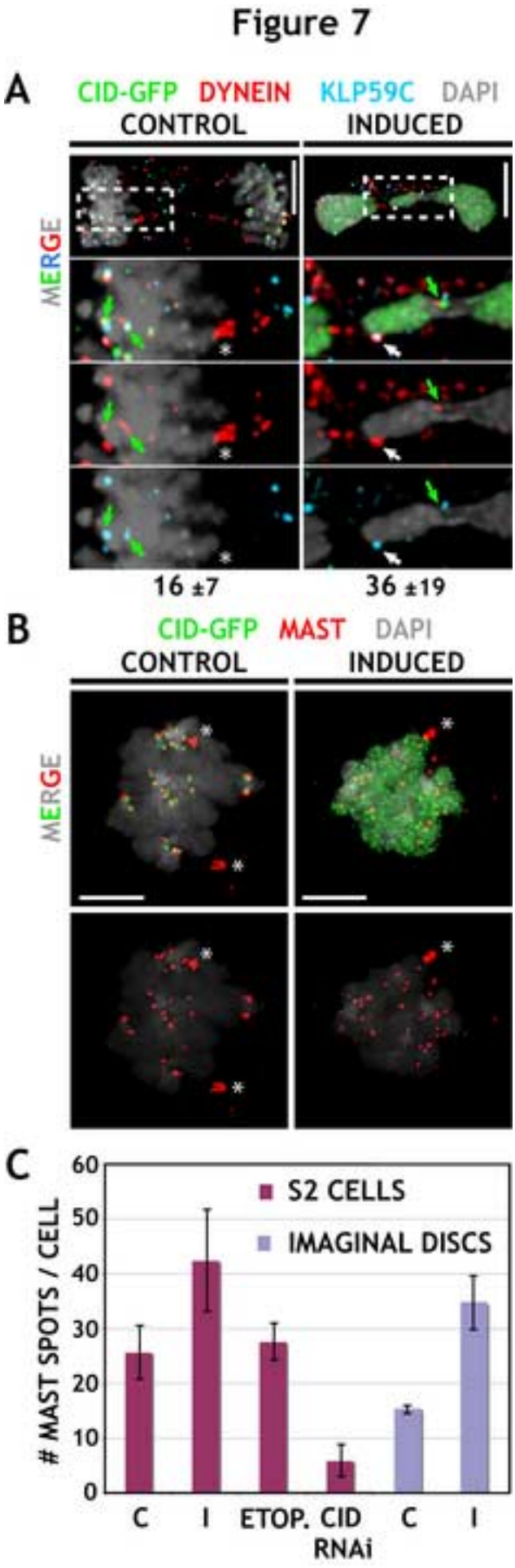

Figure 8

Click here to download high resolution image

Figure 8

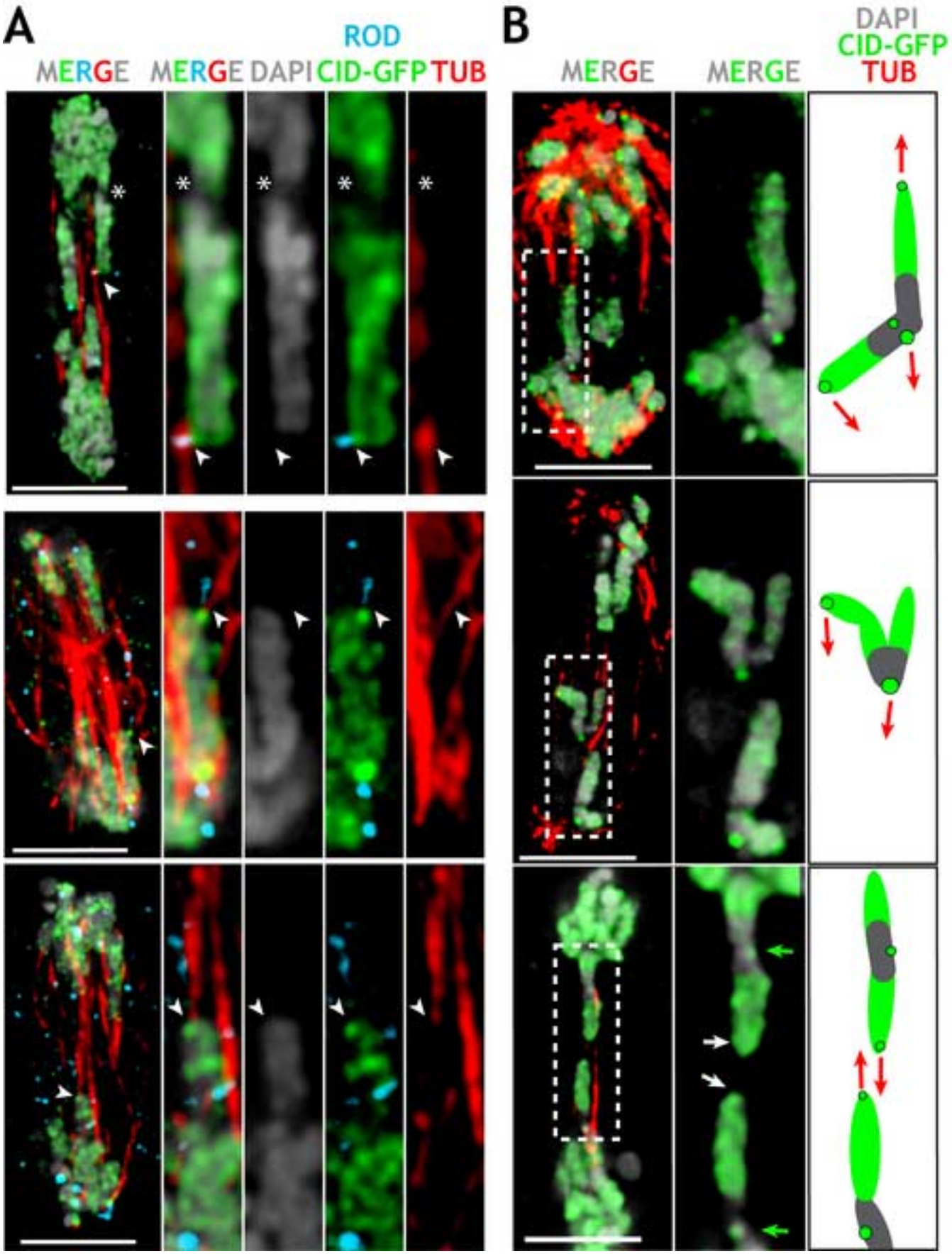

Supplemental Figure Legends

Supplemental Figure 1 Induction of CID-GFP results in significantly elevated protein levels in comparison to endogenous CID. **(A)** Western blot analysis of total cell extracts from S2 cells stably transfected with CID-GFP or H3-GFP, either induced with $CuSO_4$ (+) or uninduced (-). Expression was determined using anti-CID (short and long exposure), anti-Histone H3, and anti-GFP antibodies. One asterisk indicates degradation products of CID-GFP or H3-GFP respectively; two asterisks indicate low levels of a potential H3/H4-heterodimer. **(B)** Quantitative analysis indicated that the ratio of CID-GFP to endogenous CID was 2-fold without induction and 70-fold after induction; thus, overall induction of CID-GFP was 35-fold. H3-GFP levels without induction were negligible compared to endogenous H3 (1:350), due to the repeated nature and high expression levels of endogenous H3 genes; induction increased H3-GFP levels 27-fold, which resulted in a H3-GFP:H3 ratio of 1:13.

Supplemental Figure 2 CID overexpression elevates the mitotic index and cell death. **(A)** Eye-antenna imaginal discs from EY GAL4/ UAS-CID-V5 larvae were stained for CID (green) and a marker for mitotic cells (H3 phospho-Serine10, red). The percentage of cells in mitosis in the eye disc (10.5%) was 3.5-fold higher than in the antenna disc (3%), where CID levels are normal (n=1000). Interestingly, very strong CID overexpression was more likely to be found in mitotic cells, which suggests that these cells were arrested or severely delayed in mitosis. **(B)** Whole discs were stained with acridine orange (AO), a vital dye that stains dying but not living cells. Control discs (H3-V5) did not stain for AO, whereas induced CID-V5 cells frequently stained for AO. These observations suggest that CID overexpression triggers apoptosis, most likely due to the observed chromosome missegregation phenotypes. **(C)** Extended time-lapse analysis of live S2 cells. Frames from time-lapse microscopy are shown for two different cells with medium levels of CID-GFP (green) co-expressed with H2B-RFP (red; chromosome counter stain). One cell appeared to segregate most chromosomes prior to cytokinesis (row 1), and was able to undergo a second round of division after 24 h. In contrast, the cell in row 2 exhibited extensive mitotic defects in the first division, including chromosome stretching, fragmentation, and the cut phenotype. As a consequence, the two daughter cells did not undergo a second division, and died about 26 h later with strongly condensed chromosomes and severely altered nuclear and cellular shape. Scale bars, 20 μm in **A, B**; 5 μm in **C**.

Supplemental Figure 3 CID mislocalization produces mitotic defects. Chromosome behavior was assayed in fixed preparations from CID-GFP expressing S2 cells **(A)** and CID-V5 expressing embryos and larval discs and brains, induced by the TUB-GAL4 driver **(B)** (green=CID). Controls show normal progression through mitosis. Induction of CID expression produced stretched, lagging, and fragmented chromosomes at anaphase. The green arrow marks the endogenous centromere, and white arrows mark the corresponding phenotype. Chromosome fragments within the white box are shown at higher magnification below. The fragments contain CID, and in animals are most commonly located close to the spindle poles **(B),** suggesting that they were produced by abnormal spindle attachments. Very few mitotic defects were observed with our control (not shown). Scale bars, 5 μm.

Supplemental Movie S1 Movie corresponding to Figure 3A; row 1, 'control'. S2 cells expressing high levels of Histone H3-GFP were filmed 24 hr after induction. 7 z-stacks were taken per minute for 38 minutes and quick projected to one frame. green=Histone H3-GFP. Display is at 2 frames/sec. Scale bar, 5 μm.

Supplemental Movie S2 Movie corresponding to Figure 3A; row 2, 'control'. Uninduced S2 cells expressing low levels of CID-GFP were filmed. 7 z-stacks were taken per minute for 20 minutes and quick projected to one frame. Red= Histone H2B-RFP, green=CID-GFP, blue=transmission light. Display is at 2 frames/sec. Scale bar, 5 μm.

Supplemental Movie S3 Movie corresponding to Figure 3A; row 3, 'stretched'. S2 cells expressing high levels of CID-GFP were filmed 24 hr after induction. 7 z-stacks were taken per minute for 90 minutes and quick projected to one frame. Green=CID-GFP. Display is at 2 frames/sec. Scale bar, 5 μm.

Supplemental Movie S4 Movie corresponding to Figure 3A; row 4, 'fragmented'. S2 cells expressing high levels of CID-GFP were filmed 24 hr after induction. 7 z-stacks were taken per minute for 120 minutes and quick projected to one frame. Green=CID-GFP. Display is at 2 frames/sec. Scale bar, 5 μm.

Supplemental Movie S5 Movie corresponding to Figure 3A; row 5, 'cut'. S2 cells expressing high levels of CID-GFP were filmed 24 hr after induction. 7 z-stacks were taken per minute for 80 minutes and quick projected to one frame. Green=CID-GFP, blue=transmission light. Display is at 2 frames/sec. Scale bar, 5 μm.

Supplemental Movie S6 Movie corresponding to Figure 3A; row 6, 'Etoposide'. Uninduced S2 cells expressing low levels of CID-GFP preincubated with the Topo II inhibitor etoposide were filmed. 7 z-stacks were taken per minute for 30 minutes and quick projected to one frame. Red= Histone H2B-RFP, green=CID-GFP, blue=transmission light. Display is at 2 frames/sec. Scale bar, 5 μm.

Supplemental Movie S7 Movie corresponding to Figure 3A; row 7, 'CID RNAi'. Uninduced S2 cells normally expressing low levels of CID-GFP were pretreated with double stranded RNA to eliminated CID transcript by RNAi. 7 z-stacks were taken per minute for 76 minutes and quick projected to one frame. Red= Histone H2B-RFP, green=CID-GFP, blue=transmission light. Display is at 2 frames/sec. Scale bar, 5 μm.

Supplemental Movies S8 and S9 Movie corresponding to Figure 8A; row 1. Red= Tubulin, green=CID-GFP, transparent grey=DAPI. Shown is a 360º rotation of a volume model, directly calculated from the microtubule-chromosome arm connections displayed in Figure 8A using the model3D tool of softWoRx®.

Supplemental Experimental Procedures

Supplemental Figure 1

Total nuclear protein was prepared from stably transfected Schneider S2 cells carrying CID-GFP or H3-GFP, with (24 h) or without $CuSO_4$ induction. Proteins were separated on NuPAGE ™ 12% Bis-Tris gels (Invitrogen) using MES-buffer, pH 7.3, and processed for western blot using the Invitrogen NuPAGE® protocols. Chicken anti-CID (1:1000), rabbit anti-GFP (1:5000) and rabbit anti-H3 (1:5000) were used for primary detection, followed by corresponding secondary-antibodies coupled with horseradish peroxidase (1:5000). Blots were developed using ECL-plus (Pharmacia/Amersham), signals were captured using a Chemidoc XRS (BioRad), and band intensities were quantified with the Quantity One® software (BioRad).

Supplemental Figure 2

Acridine orange staining was performed as described (McCall and Peterson, 2004). To capture consecutive cell cycles by live imaging of the same cell (Supplemental Figure 2C), protein expression was pulse-induced in 1ml of 1x106 cells/ml growing cell culture using 250 mM CuSO4 for 12 hours. Induction medium was than replaced by normal medium (chase). Cells were resuspended and 100 µl was plated into a custom made growth chamber slide, consisting of 6 individual chambers mounted on a regular glass slide with 6 holes and a cover slip bottom. Time-lapse microscopy of <1 hour was

performed on cells with low and high levels of CID-GFP in metaphase as described before. After 24 hours and 48 hours the same cells were imaged again with a frame rate of 1 frame/5 min for 4 hours. Cells grew with normal kinetics for at least 3 days under these conditions before they require a medium change.

Supplemental Figure 1

A

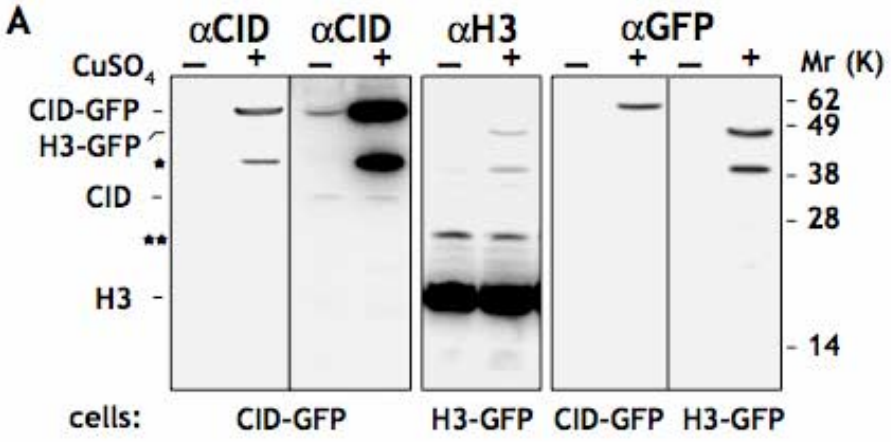

B

	- $CuSO_4$	+ $CuSO_4$	Induction
CID-GFP : CID	2:1	70:1	35 fold
H3-GFP : H3	1:350	1:13	27 fold

Supplemental Figure 2

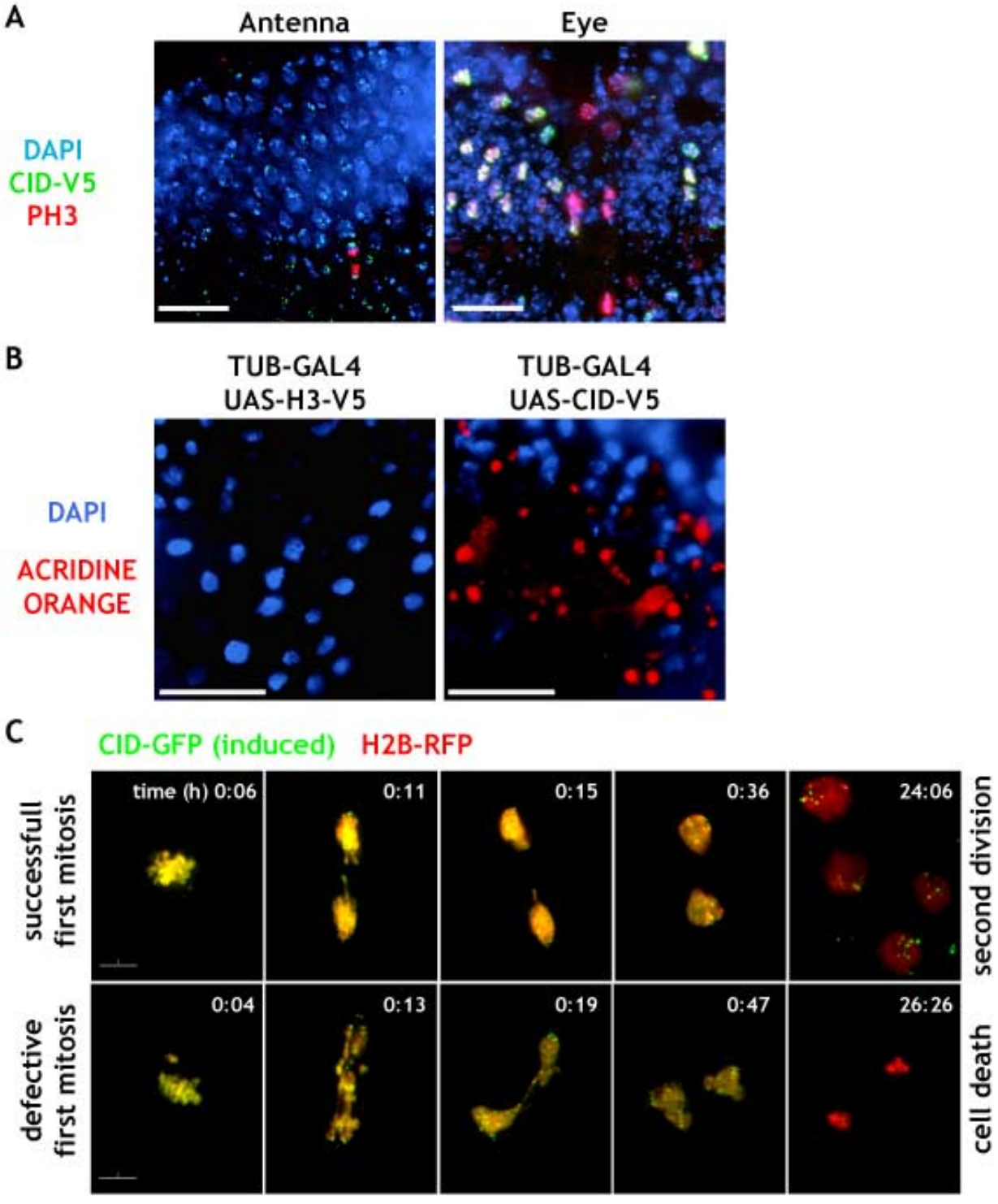

Supplemental Figure 3

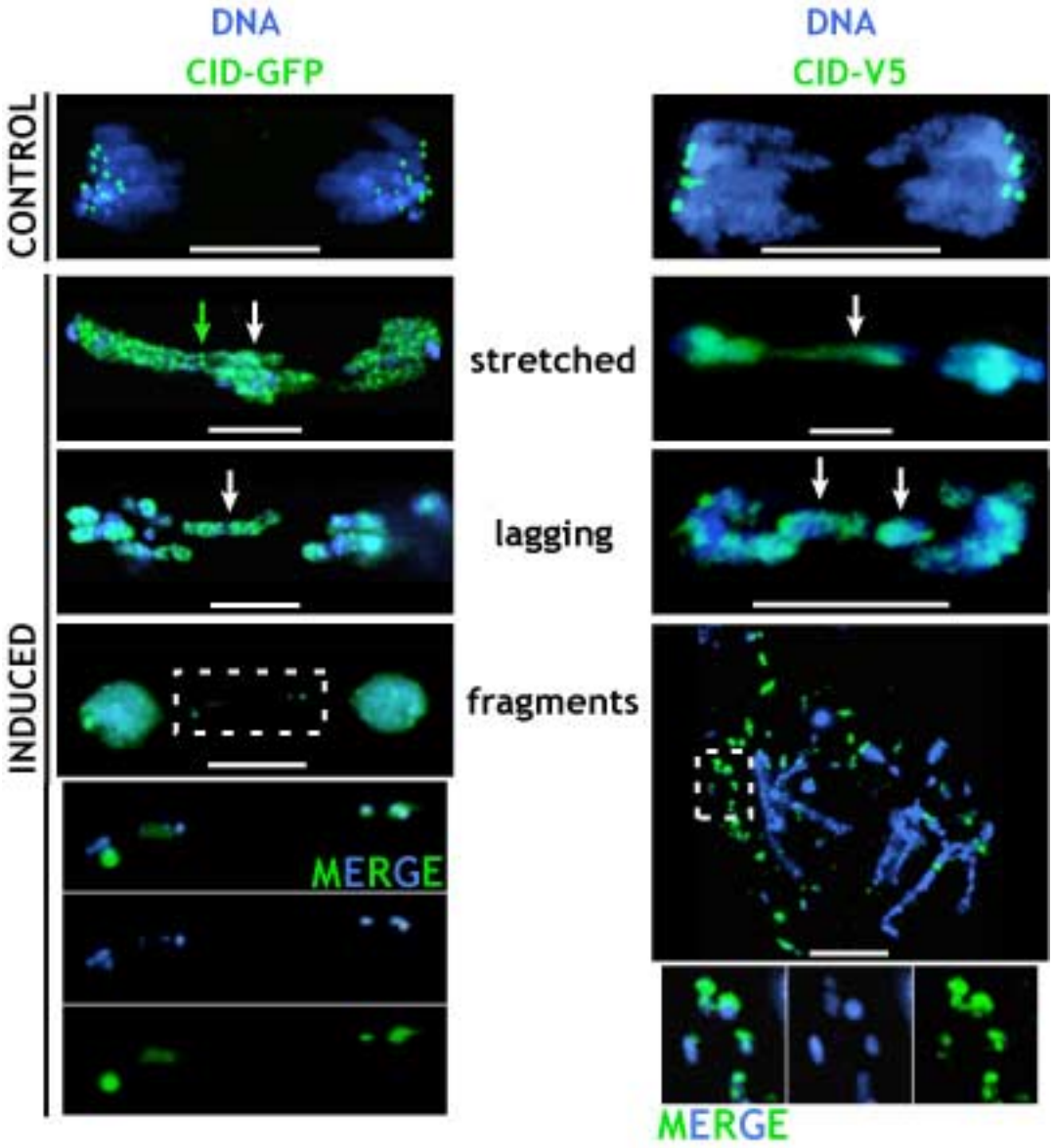

Supplemental Tables

Supplemental Table 1: Ectopic localization of kinetochore proteins in S2 cells

Protein 1	Protein 2	# SPOTS / NUCLEUS (AVG ± SD)								
		1			2			1 + 2		
		C	I	fold ┌	C	I	fold ┌	C	I	fold ┌
CENP-C		26 ±4	71 ±11	2.7	-	-		-	-	
MEI-S332		29 ±4	49 ±9	1.7	-	-		-	-	
BUBR1		26 ±3	44 ±9	1.7	-	-		-	-	
CENP-C	MEI-S332	30 ±4	72 ±6	2.4	32 ±5	61 ±7	1.9	22 ±4	43 ±6	2.0
CENP-C	POLO	30 ±7	75 ±12	2.5	27 ±5	59 ±9	2.2	22 ±4	40 ±4	1.8
ROD	POLO	32 ±5	46 ±8	1.4	30 ±4	51 ±7	1.7	27 ±3	39 ±3	1.4
MEI-S332	BUBR1	34 ±3	66 ±10	1.9	26 ±4	49 ±8	1.9	17 ±2	26 ±8	1.5
DYNEIN	KLP59C	39 ±12	56 ±26	1.4	41 ±13	77 ±35	1.9	16 ±7	36 ±19	2.3

C= control, I=induced

Supplemental Table 2: Ectopic localization of kinetochore proteins in disc cells

Protein 1	Protein 2	# SPOTS / NUCLEUS (AVG ± SD)								
		1			2			1 + 2		
		C	I	fold ┌	C	I	fold ┌	C	I	fold ┌
CENP-C		16 ±1	53 ±10	3.3	-	-		-	-	
MEI-S332		19 ±4	42 ±13	2.2	-	-		-	-	
BUBR1		16 ±2	31 ±5	1.9	-	-		-	-	
CENP-C	MEI-S332	16 ±1	58 ±7	3.6	16 ±1	51 ±7	3.2	16 ±1	45 ±7	2.8
CENP-C	POLO	16 ±1	54 ±10	3.4	16 ±2	42 ±11	2.6	16 ±2	40 ±11	2.5
ROD	POLO	17±3	35±6	2.1	17±5	36±15	2.1	15 ±2	26 ±3	1.7
MEI-S332	BUBR1	16 ±1	43 ±9	2.7	16 ±1	39 ±11	2.4	16 ±1	38 ±12	2.4

C= control, I=induced